applied sciences

MDPI

Article

Modeling and Evaluation of Oxy-Combustion and In Situ Oxygen Production in a Two-Stroke Marine Engine

José R. Serrano [1], Francisco J. Arnau [1,*], Alejandro Calvo [2] and Rossana Burgos [1]

[1] CMT-Clean Mobility&Thermofluids, Universitat Politècnica de València, 46022 Valencia, Spain; jrserran@mot.upv.es (J.R.S.); prburque@posgrado.upv.es (R.B.)
[2] Wärtsilä Services Switzerland Ltd., 8500 Frauenfeld, Switzerland; alejandro.oliveira@wartsila.com
* Correspondence: farnau@mot.upv.es; Tel.: +34-96-387-6500

Abstract: Considering the concerns for emissions reduction in the maritime sector, the present paper evaluates, through modeling and simulation, oxy-fuel combustion in a two-stroke ship engine (2SE) and the best production system configuration to obtain the required oxygen (O_2). An initial model of a ship engine is calibrated with the engine manufacturer's data and then adapted to work with O_2 as the oxidant to eliminate nitrogen oxide (NO_x) emissions and with exhaust gas recirculation (EGR) to control the in-cylinder combustion temperature. Mixed Ionic–Electronic Conducting (MIEC) membranes produce the necessary O_2 from the ambient air, which is heated up and pressurized by a heat exchanger and turbocharging coupled system to provide the air conditions required for the proper operation of the MIEC. Several layouts of this system are evaluated for the full load engine operating point to find the optimum O_2 production system configuration. Results reveal that the engine operating under oxy-fuel combustion conditions avoids NO_x emissions at the expense of higher brake-specific fuel consumption (BSFC) to obtain the original brake torque, and also expels a stream composed exclusively of CO_2 and H_2O, which facilitates the separation of CO_2 from exhaust gases.

Keywords: internal combustion engine; maritime transport; oxy-fuel combustion; MIEC; turbocharging

Citation: Serrano, J.R.; Arnau, F.J.; Calvo, A.; Burgos, R. Modeling and Evaluation of Oxy-Combustion and In Situ Oxygen Production in a Two-Stroke Marine Engine. *Appl. Sci.* **2023**, *13*, 10350. https://doi.org/10.3390/app131810350

Academic Editor: Wenming Yang

Received: 6 August 2023
Revised: 8 September 2023
Accepted: 12 September 2023
Published: 15 September 2023

1. Introduction

Shipping is the main freight transport mode around the world, transporting about 90% of global trade. Although it is the least atmosphere-damaging means of transport, its cumulative effect contributes to the overall air quality problem [1]. The International Maritime Organization (IMO) is the United Nations' regulatory agency for safety, security, and environmental performance of the shipping industry. IMO controls the reduction of major ship exhaust emissions (SO_x, NO_x, VOCs, and ODS) through Annex VI of the International Convention for the Prevention of Pollution from Ships (MARPOL) [2]. This regulation reduces the global SO_x limit to 0.50% m/m outside an Emission Control Area (ECA), and to 0.10% m/m inside, and it regulates the NO_x emissions through three tiers based on the ship construction date and the engine speed, as indicated in Table 1 [3]. Concerning the CO_2 emissions from ships, IMO adopted an Initial Strategy, still pending review in 2023, whose main goal is to cut annual GHG emissions by at least half by 2050 compared with their level in 2008 [4].

Table 1. Total weighted cycle NO_x emission limit [g/kWh] for ship engines [3].

Tier	Construction Date	$n < 130$	$n = 130–1999$	$n \geq 2000$
I	1 January 2000	17.0	$45 \times n^{-0.2}$	9.8
II	1 January 2011	14.4	$44 \times n^{-0.23}$	7.7
III	1 January 2016	3.4	$9 \times n^{-0.2}$	2.0

Currently, there are three reduction strategies for marine engines in order to meet the SO_x and NO_x emission standards on ships: fuel optimization, pre-combustion control, and exhaust after-treatment systems. Fuel optimization consists of replacing heavy ship fuels, such as heavy fuel oil (HFO) and marine diesel oil (MDO), with clean alternative fuels to mitigate SO_x and PM emissions due to low sulfur content; pre-combustion control techniques, such as water addition and EGR, are adopted for controlling NO_x emissions by preventing its formation conditions during combustion; and the exhaust after-treatment systems, among them SCR to decrease NO_x and DPF to remove PM, are technologies that effectively reduce NO_x and PM emissions without significant penalty in the engine power and fuel economy [5].

Intending to reduce their environmental footprint, the shipping industry is switching to cleaner fuels, either by replacing fossil fuels with low-carbon and carbon-negative fuels, or by using carbon-neutral fuels [6]. However, a technology to decrease CO_2 emissions is still necessary to meet the global objective of the Paris Agreement; Carbon Capture and Storage is one of the key technologies for this purpose. In CCS, the CO_2 is captured in three ways—post-combustion capture, pre-combustion capture, and oxy-combustion—and then transported to permanent offshore storage via pipeline, ship, or both [7]. As an alternative to storing the captured CO_2, it is also used during the processing of synthetic and low-carbon fuels together with green H_2 [8].

As an alternative to NO_x emission-reducing technologies and complementary to CCS, oxy-fuel combustion appears as a novel option. In this combustion process, air is replaced by high-purity oxygen to eliminate NO_x emissions by the absence of N_2, obtaining as exhaust gases mainly CO_2 and H_2O, which are used to control the high combustion temperature [9]. Oxy-fuel combustion facilitates the separation of CO_2 from H_2O after condensation, so this concept was initially implemented in power plants, both coal-fired [10] and biomass-fired [11], as an alternative to the Carbon Capture and Storage (CCS) methods of post-combustion and pre-combustion [12]. Environmental concerns about CO_2 emissions to the atmosphere from energy-intensive industries have promoted the study and implementation of oxy-fuel combustion in sectors such as oil refining [13], IGCC systems [14], and cement production [15]. In addition to CO_2 sequestration, oxy-fuel combustion is used, due to its high combustion temperature, for processes like High-Velocity Oxy-Fuel (HVOF) coating [16] and Basic Oxygen Furnace (BOF) for steel production [17].

The oxygen supply is the biggest challenge for oxy-fuel combustion in engines since it is not readily available in the environment and must, therefore, be obtained in another way. Offboard acquisition is a challenging option, as it entails additional storage and transport costs, and mainly because of the weight and space limitation in vehicles, which reduces the autonomy essential for means of transport such as airplanes and ships. On the other hand, in situ O_2 production techniques are foreseen to be a promising solution in the near future. Under this category, the production of O_2 via a cryogenic air separation unit (C-ASU) is the most developed technology, as it provides large quantities of high-purity oxygen. However, extensive capital investments and energy demand [18] make its implementation difficult in oxy-combustion processes [19]. As an alternative, the Oxygen Transport Membranes (OTMs), also known as Mixed Ionic–Electronic Conducting membranes (MIEC), present an energetic and economic advantage compared to C-ASU [20].

MIEC membranes rely on O_2 diffusion through the crystal lattice of the membrane material [21] caused by the O_2 partial pressure difference between the feed and permeate sides of the membrane (see Figure 1) [22]; for this reason, the selectivity of the membranes is superior to other technologies and it is possible to obtain high-purity oxygen [23]. The driving force that moves O_2 through the membrane can be achieved in two different ways: the 3-end design that generates a vacuum in the permeate side, and the 4-end design that reduces the partial pressure of O_2 on the permeate side with a sweep stream of recirculated flue gas. Although the second option increases the energy efficiency of the process, the membrane is exposed to species such as CO_2, SO_2, H_2O than can deteriorate it. Regarding the membrane material, perovskites are the most commonly used for membrane manufac-

turing because they provide high oxygen flux; however, they are prone to poisoning when they come in contact with CO_2 and SO_2 [20]. BSCF is one of the perovskite materials which presents higher O_2 permeability [24], and it is important to consider that below 850 °C, the perovskite does not present the same permeation capability [20].

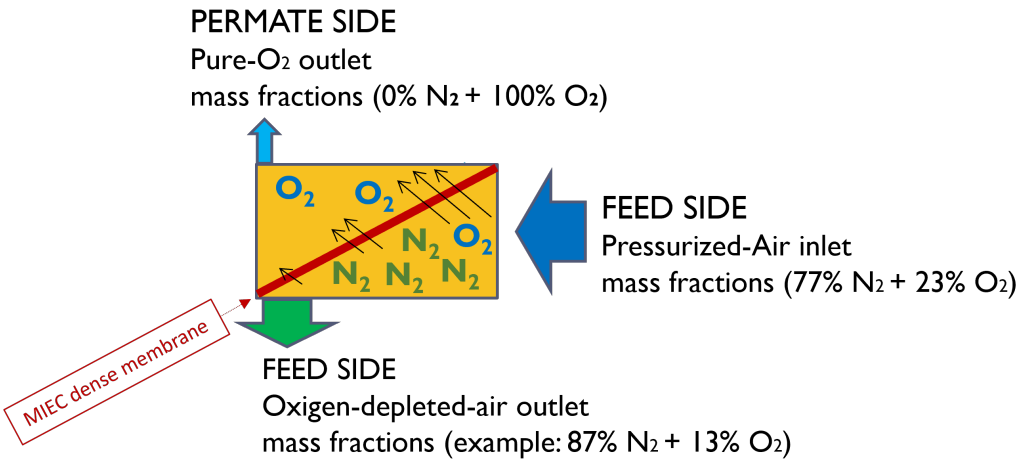

Figure 1. Schematic representation of MIEC oxygen permeation.

The study of oxy-fuel combustion technology in ship engines is still very new. The only research project in progress is RIVER, led by the education group YNCREA Hauts de France and co-financed by the European Union within the Interreg North-West Europe program. The objective is the reduction of NO_x and CO_2 emissions from inland waterway vessels applying oxy-fuel combustion and CCS technology for diesel engines [25]. In this project, the oxygen is made available in cylinders that contain high-pressure oxygen and are located in a safety lifting cage in the narrowboat. This system has the capacity to supply O_2 for about one hour depending on the load and speed of the vessel, so refilling of the cylinders must be carried out by a mobile crane located on the dock [26]. The ultimate goal of the RIVER project is the installation and integration of the oxy-fuel combustion system with CO_2 capture and storage on a narrowboat operating on UK inland waterways in real conditions [27]. As part of this project, a CFD study was carried out to evaluate the influence of different diluent strategies for the oxy-fuel combustion process in a High-Speed Direct Injection (HSDI) diesel engine under Homogenous Charge Compression Ignition (HCCI) mode [28].

Oxy-fuel combustion in the engines of large marine vessels is not comparable to the case mentioned above, since the environmental and operating characteristics between inland waterways and ocean-going ships are different. Furthermore, an on-site oxygen supply is necessary for maritime transport due to the large quantities of oxygen required by the engine and the far distances to land, as opposed to inland waterway transport. Thus, the present study explores these issues by modeling an oxy-fueled ship engine and designing the most optimal system for it.

2. Method

This research was carried out with the following steps:

- In the first instance, the baseline engine model was configured in the gas dynamics simulation tool to be used during the study.
- The second step was the implementation of the oxy-fuel combustion in the model, aiming to achieve an engine performance close to the original.
- Finally, the in situ oxygen production system was designed separately from the main engine model.

The model developed by the authors has been built into the in-house platform software called VEMOD (Virtual Engine MODel). VEMOD is a gas dynamics software for simulation

of reciprocating internal combustion engines. It is a 1D and 0D simulation software that accounts for gas dynamics in pipes and volumes of internal combustion engines, solving Euler's set of equations of mass, momentum, and energy conservation by finite volume numerical techniques. They all account for many boundary conditions, such as submodels for reciprocating internal combustion engines. These include combustion inside cylinders, the crank-resolved gas exchange process of cylinders, turbocharging, heat exchangers, and other engine elements. All of them are fast enough to be close to real-time calculation. Therefore, even with crank angle resolution, they can solve many engine cycles and transient processes of reciprocating internal combustion engines. For the sake of brevity and since the main purpose of the paper is not detailing the insights of these complex typology of simulation platforms, we direct the interested reader to [29], so those interested in further insights can read more about the details of the in-house software VEMOD from the CMT Research Institute of UPV, which includes non-stationary calculation in one-dimensional conditions of flows of different gases, stationary and zero-dimensional calculation of cooling and lubrication systems, nodal calculation of heat transmission in engine cylinders considering thermal transients, the possibility of simulating reciprocating engines' stationary or transient operating conditions with angular resolution, and additional elements, including heat exchangers, turbocharging groups, gas cleaning systems (aftertreatment), air filters, fuel injection systems, etc. The possibility of also being used for the non-stationary calculation of complex gas piping systems driven by radial turbomachines is also discussed. The virtual engine model has been validated with experimental tests on a 1.6 L diesel engine through stable and transient tests under hot and cold conditions. The engine torque was predicted with a mean error of 3 Nm and an error of less than 14 Nm for 90% of the cycle duration. CO_2 presented an average error of 0.04 g/s, while during 80% of the cycle, the error was less than 0.44 g/s. VEMOD is programmed in C++.

2.1. Configuration of the Baseline Model

The marine engine evaluated in this study is a two-stroke, 8-cylinder CI engine, diesel-fueled by direct injection. Its reference name is 8X82-2.0 with the standard configuration 'Delta-Bypass-Tuning'. Experimental data for 8X82-2.0 can be found at the website [30]. All data available on the web referring to the 8-cylinder X82-2.0 diesel engine model apply to the baseline configuration of the present paper. More data can be found in the open software GTD.exe, which can be downloaded from the tab General Technical Data (GTD) [31] at the referred website and using the standard configuration 'Delta-Bypass-Tuning'. These data correspond to torque and power in dimensionless format, further used in paper figures. The dimensionless chart design has been preferred for brevity in the number of charts, for better comparison among different series and generality of the presentation of the obtained results. Authors consider the dimensionless chart format quite convenient because similarity laws work well for reciprocating engines, and trends can be extrapolated to other cylinders or geometrical dimensions.

The engine manufacturer provided a reference model of the ship propulsion system in 1D-0D gas dynamics software, which solves Euler equations by finite volume schemes and can be found within the GT-SUITE™ v2021 software package from Gamma Technologies™ (Westmont, IL 60559, USA). In addition to the engine, the reference model includes a turbocharger, a water CAC, and an electric auxiliary blower for each of four cylinders, as shown in Figure 2a. To obtain the base engine behavior for this study, the simulations were run at different operating points (presented in Table 2) and controlling the injection fuel to reach the BMEP target.

This model was replicated in the simulation software 0D-1D Virtual Engine Model (VEMOD) [29] developed by the research institute CMT—Clean Mobility&Thermofluids. This platform was selected because of the availability of the sub-models required to simulate the oxygen production stage and the versatility of the code, being the in-house code for developers capable of adapting the tool, as per the needs of the project. The VEMOD

engine model was calibrated with the ship manufacturer's virtual model to obtain similar results; for this purpose, the turbocharger speed was fixed to facilitate the tuning, then the corresponding multipliers and coefficients were modified to adjust the engine operative curves, and afterward, the exhaust pressure was fine-tuned by controlling the pressure at the turbine outlet. Finally, the turbocharger speed was again released and let to rotate according to the engine operating point.

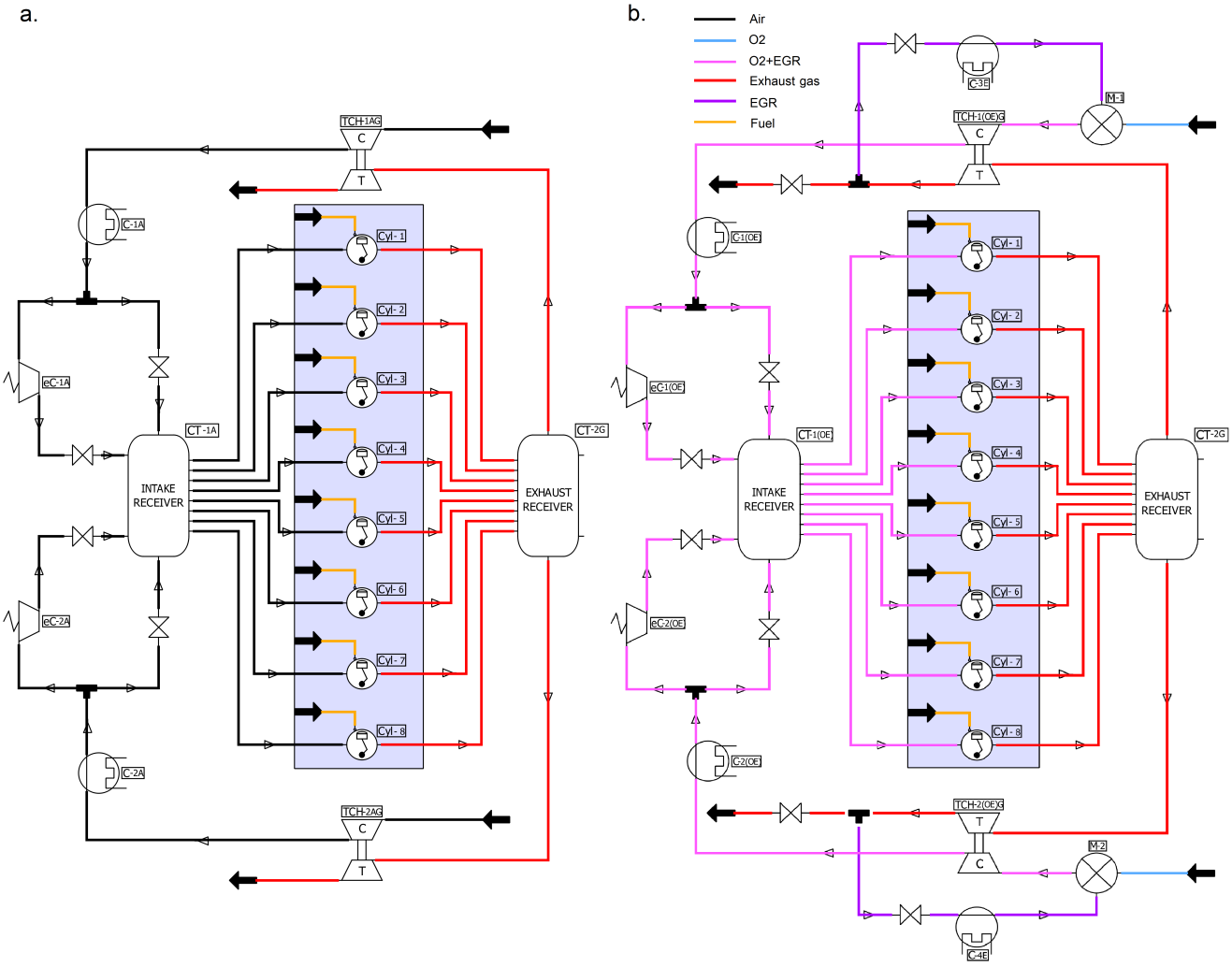

Figure 2. Marine engine models. (**a**) Baseline model. (**b**) Oxy-fuel combustion model.

Table 2. Operating points of the studied marine engine.

Engine Speed [rpm]	Load [%]
50	25
63.5	50
72.7	75
78	100

Figure 3 compares the manufacturer's model in GT-SUITE^{TM} and the authors' model in VEMOD after calibration of the VEMOD model according to the main engine performance curves and turbocharger maps. Therefore, "VEMOD" should be understood as "Baseline design—VEMOD simulations", and "Manufacturer" should be understood as "Baseline design—Manufacturer simulations". Absolute data can be found in the open software GTD.exe, which can be downloaded from the tab General Technical Data (GTD) [31] at the website [30], and using the standard configuration 'Delta-Bypass-Tuning'. These

data correspond to torque and power in the dimensionless format shown in Figure 3. The dimensionless chart design has been preferred for brevity in the number of charts, for better comparison among different series and generality of the presentation of the obtained results. Authors consider the dimensionless chart format quite convenient because similarity laws work well for reciprocating engines, and trends can be extrapolated to other cylinders or geometrical dimensions. The values were divided by the maximum value of the corresponding parameter to make the dimensionless figures. Power and Torque charts in Figure 3a are superimposed, since the values are objectives imposed to the VEMOD equal to those of the engine manufacturer model. Also, they are equal to experimental data of the 8X82-2.0 engine since the torque and power design objectives were fully achieved. The fitting shown in Figure 3b,c corresponds to turbine and compressor maps and is also very good between the manufacturer's model in GT-SUITE^{TM} and the authors' model in VEMOD. Turbine and compressor maps are formed by characteristic lines of reduced variables obtained from experimental data measured by the turbocharger supplier in a gas stand. Reduced variables simplify dimensionless variables obtained from the theorem Pi of Vaschy-Biuckingham. The reduced variables show experimental data from a full map of the operation of a single turbomachinery that always works with the same fluid type. Experimental characteristic lines collapse for the different turbocharger reduced speeds of the axial turbine in Figure 3b, in the pressure ratio vs. reduced mass flow chart. This is not the case in the compressor map shown in Figure 3c, where colorful lines show the different iso-speeds, and one can see that the higher reduced speeds reach higher pressure ratios. Due to iso-speed lines not collapsing in Figure 3c, plotting the iso-efficiency contour lines in the same map is a usual technique. One can see the contour lines in Figure 3c where white contours correspond to the highest efficiency, and it reduces as contours get darker, until minimum efficiency is reached at black contours. This level of fitting is considered adequate to use this model as a baseline for the oxy-fuel combustion study. One can even see that better results are shown with VEMOD in the case of Figure 3b, since VEMOD results fit better the turbine supplier map than the manufacturer results for low engine speeds, showing a better turbine modeling practice. The same can be said of the compressor map in Figure 3c, since the point at 50 rpm from VEMOD is well within the map operative area, whereas in the model from the manufacturer, the operative point is slightly beyond the surge limit. With these results, it can be concluded that the VEMOD model baseline is a robust one to go ahead with the oxy-fuel combustion study.

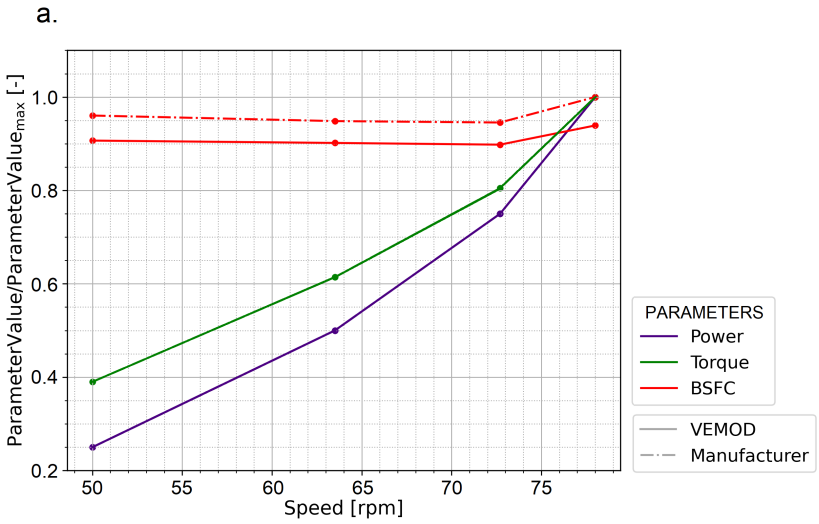

Figure 3. *Cont.*

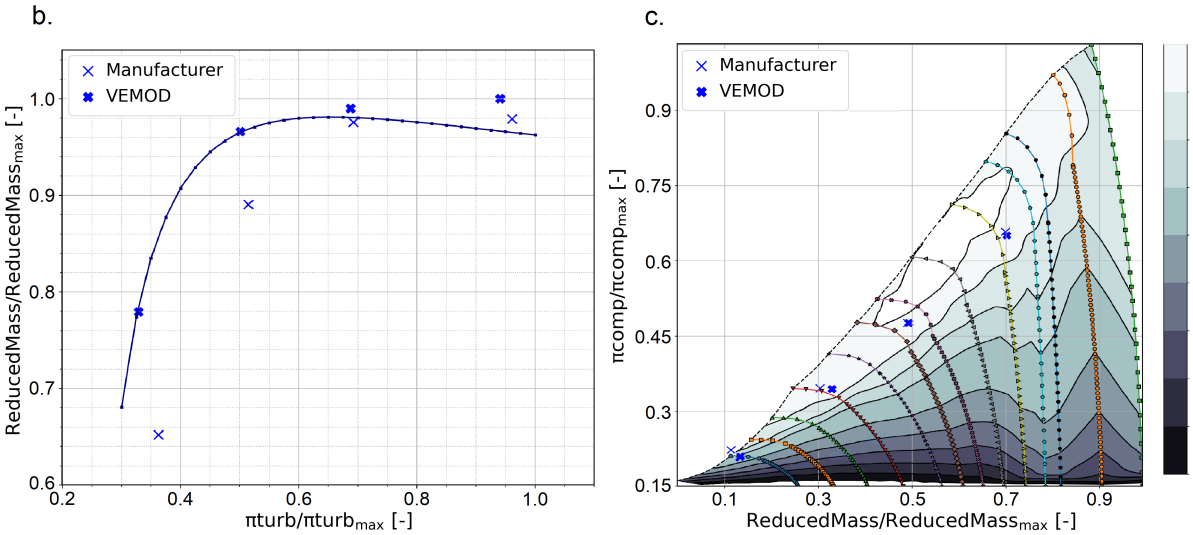

Figure 3. Comparison between manufacturer's reference model and VEMOD calibrated model. (**a**) Engine performance. (**b**) Turbine map. (**c**) Compressor map. "VEMOD" should be understood as "Baseline design—VEMOD simulations" and "Manufacturer" should be understood as "Baseline design—Manufacturer simulations".

2.2. Implementation of the Oxy-Fuel Combustion

Initially keeping the baseline model layout and the same BMEP target, the air was replaced by a mixture of O_2 and EGR, the first to incorporate the oxy-fuel combustion idea and the second to control the combustion temperature. The proportion of O_2 and EGR ($CO_2 + H_2O$) in the mixture was imposed in such a way to imitate the oxygen concentration of atmospheric air in the intake charge mixture, in order to maintain the stabilization of oxy-fuel combustion flames. These criteria have been adopted from a previous study of partially premixed CH_4/oxy-fuel flames in a swirl stabilized burner [32].

After achieving a suitable engine behavior with the imposed oxidant composition, the O_2 inlet and EGR line were configured in the model. For the first, an O_2 deposit at atmospheric conditions was included at the turbocharger inlet to represent the O_2 produced by the system to be designed later; for the EGR, the exhaust gases coming out of the turbine were divided into two lines, one leading part of the gases to the environment (where a CCS is foreseen in the next stage), and the other leading the rest to the engine intake. The EGR flow is controlled through a valve to reach the established O_2/EGR ratio, and it is refreshed by a cooler before entering the mixer, where O_2 and EGR converge before entering the compressor (see Figure 2b).

2.3. Design of the O_2 Production System

Once the engine model worked correctly with the O_2 inlet and EGR line, the O_2 production system was designed separately from the main engine scheme to facilitate the simulations, whereby the boundary conditions of the system were imposed from the engine model at full load operating point.

2.3.1. Reference Layout

The design of the O_2 production system consists of conditioning the atmospheric air to reach the operating parameters of the MIEC, since it requires feeding air at high temperature and sufficient O_2 partial pressure gradient between the feed and permeate side; for this purpose, heat exchange and turbocharging systems are necessary to heat and pressurize the inlet air.

As the starting point for the design, the layout for a direct injection CI engine developed by J.R. Serrano et al. [33] was implemented and adapted to the needs of the ship

engine model. Their proposed system uses a 4-end design membrane to improve the driving force by diluting the permeated O_2 with the engine EGR. In terms of obtaining the air conditions for the correct operation of the MIEC, on one side, the required feed air pressure is achieved by means of a regenerative Brayton cycle with two stages of compression and expansion, in which the MIEC represents the combustion chamber in a conventional cycle, and the turbines are driven by the N_2 leaving the MIEC. On the other side, the required temperature is obtained through a Heat Exchanger Network distributed to recover the energy from the exhaust gases coming from the engine, and from the N_2 and O_2 leaving the MIEC at very high temperatures. A membrane area study is carried out to determine the minimum area capable of supplying the required oxygen, depending on the air conditions achievable by the O_2 production system. The referred article [33] shows and explains in detail this oxy-fuel engine proposal with in situ O_2 production.

2.3.2. Layout Conception

An initial O_2 production model was designed considering the main elements of the reference layout and the marine engine conditions. For this case, a 3-end design membrane was used to produce the O_2 because the sulfur content in ship engine fuels is too high and the EGR could poison the membrane, which means that the sweep stream was eliminated and another way to increase the driven force in the MIEC is needed. To obtain this force, the Brayton cycle was modified. Instead of two stages of compression and expansion, one turbocharger compresses the inlet air and the other extracts the outlet O_2 from the membrane to generate a vacuum in the O_2 line, and thus, the partial pressure gradient required in the MIEC is obtained. The turbochargers, the sizes of which remain unchanged to those of the engine model, were placed in parallel to simplify the control in this initial system's conception.

As for the Heat Exchanger system, it still recovers the residual energy of the N_2 and O_2 from the MIEC, but unlike the reference model, the energy of the exhaust gases is not enough to reach the target air temperature since the marine engines expel the post-combustion gases at temperatures around 400 °C and with excess O_2. The solution strategy for this energy shortage was adding a combustion chamber in the exhaust gases and EGR lines to take advantage of the remaining O_2 in the gases and thus increase the heat transferred to the air; the fuel injection of the combustion chambers is controlled to produce an amount of oxygen equal to the demand of the engine at full load. Furthermore, the EGR line is split with a dual purpose: harnessing the energy of the O_2 and exhaust gas flow lines to heat up the air and cooling both to facilitate the future processes, i.e., O_2 compression in the engine model and CO_2 capture, which will be incorporated in a future study.

The membrane selection was based on the study performed during the design of the reference layout, first by scaling the membrane areas evaluated as a function of the O_2 needs, and then locating the minimum required for the most achievable conditions in the MIEC estimated for this study. Since there is not sweep current this time, it is more difficult to obtain a high O_2 partial pressure ratio, so the membrane area selected as a first approximation was 6000 m^2, which is the minimum area needed to produce the required O_2 at the minimum O_2 partial pressure ratio in the MIEC. This first attempt at configuring the O_2 production system is depicted in Figure 4.

2.3.3. Layout Optimization

To achieve the most energy-efficient model, the O_2 production system was optimized to meet the next condition: achieve the lowest possible fuel consumption in the burners to produce the O_2 required for the oxy-fuel combustion engine. This optimization process was carried out on the turbocharging system and MIEC membrane.

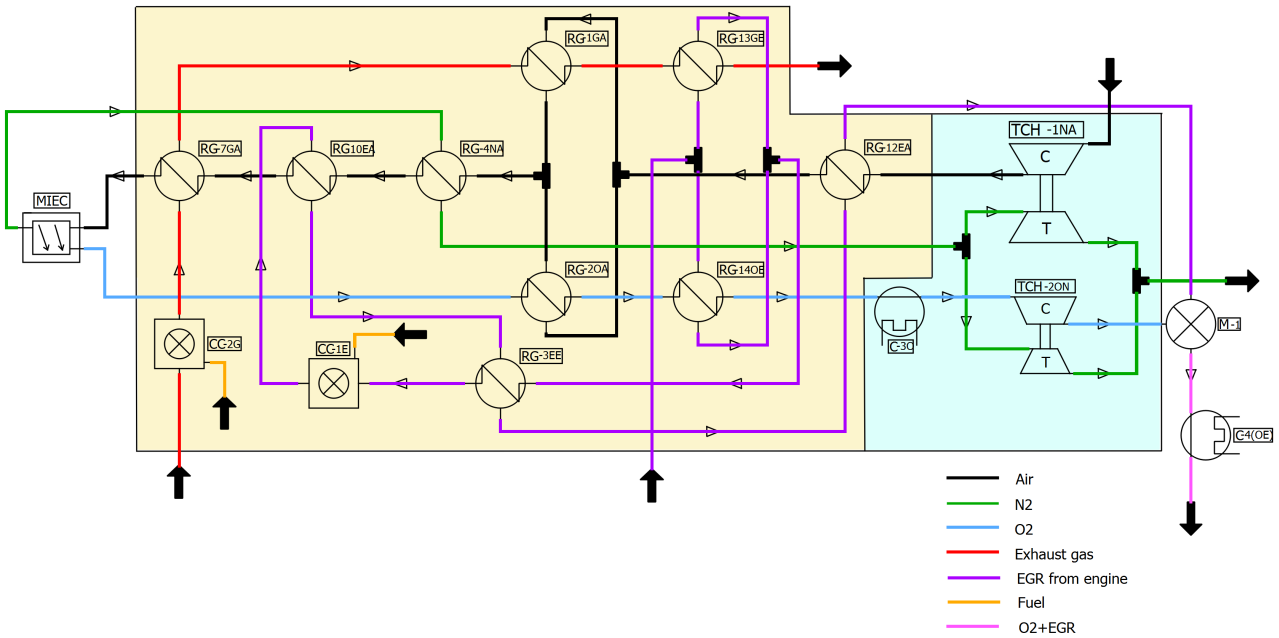

Figure 4. O_2 production system with parallel turbocharging system.

Turbocharging System

Different turbocharging setups were analyzed to find the configuration that best meets the established optimization parameter. The study conducted for each arrangement was carried out as follows. Maintaining the size of the turbocharger receiving air from the atmosphere, i.e., TCH-1NA in Figures 4–6, a sweep of the size scale factor of the second turbocharger is performed, i.e., TCH-2ON in Figures 4 and 5, and TCH-2NA in Figure 6. Simultaneously with the previous point, the corrected mass flow factor of the compressor, corresponding to each scale factor, is adjusted to operate in the most efficient island of the map. Finally, the fuel consumption of the burners obtained along the sweep is used as the objective function to find the best size ratio between the turbochargers.

At the end of this stage, the best turbocharging configuration for the final O_2 production model is selected. Each of the layouts studied is explained below.

- *Parallel configuration:* The first turbocharging proposal consists of connecting two units in parallel with a common N_2 line at the inlet of the turbines. The TCH-1NA turbocharger is placed at the beginning of the air flow line and the TCH-2ON turbo at the end of the O_2 line to achieve the required O_2 partial pressure gradient in the MIEC. This parallel configuration is shown in the light blue box in Figure 4.
- *Serial configuration:* Maintaining the location of the turbochargers in the scheme, the second turbocharging attempt was a series turbine configuration in which the N_2 line is regulated by a bypass valve to first drive the TCH-2ON turbine and then, when the N_2 flow confluences again, drive the TCH-2ON turbine. The bypass valve lift was swept to determine the best possible value. This serial configuration is shown in the light blue box in Figure 5.
- *Two-stage air compression:* The third configuration analyzed was another serial arrangement, but in this case for both turbines and compressors. The air is compressed twice to further increase the partial pressure gradient in the MIEC without the need to generate vacuum. This configuration is shown in the light blue box in Figure 6; the heat exchanger system is different from that shown in the previous figures because, as will be demonstrated in the results section, the EGR line burner is not necessary for this setup at full engine load.

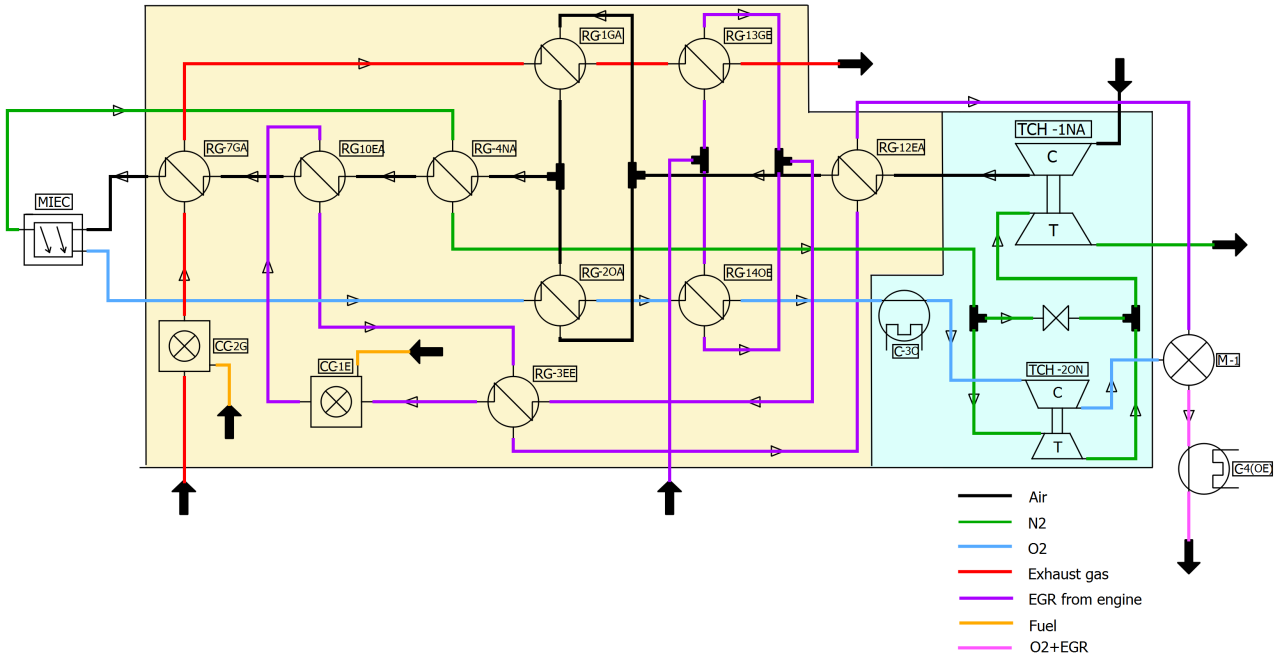

Figure 5. O_2 production system with serial turbocharging system.

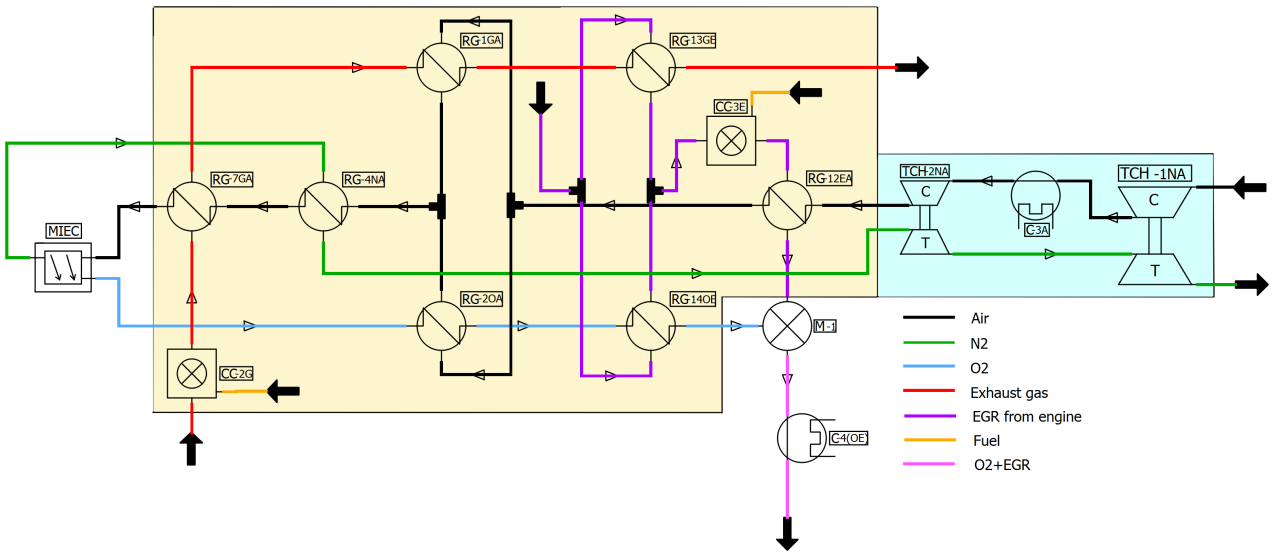

Figure 6. O_2 production system with two-stage air compression system for all engine operating points.

The latter option, which is the best of the three turbocharging systems (justification in Section 3), was adapted to work at all other engine operating points. The study shows that, in order to reach the required air conditions in the MIEC, the incorporation of the EGR burner line is only necessary at the two lowest engine load points. This addition is represented in Figure 6.

MIEC Membrane

As indicated in the description of the layout conception, the membrane area initially selected for the design of the O_2 production system was 6000 m^2. It is worth mentioning that a sweep of the membrane area was performed and will be presented in the results section with the aim of obtaining the optimal membrane area for the O_2 production system.

3. Results and Discussion

This section describes and discusses the ship engine behavior under oxy-fuel combustion conditions and the outcome of the O_2 production system design. As explained in the method section, the values of the parameters are shown as the ratio to the maximum value since the engine data are confidential information of the manufacturer; for this reason, the results are analyzed considering the tendency and the rate of change of the variable, not its magnitude. Several parameters are plotted on the same graph to directly analyze their relationship with each other, and a standard color code is used for each property to simplify the reading of the figures.

3.1. Engine Behavior under Oxy-Fuel Combustion

Replacing N_2 with EGR (CO_2 and H_2O) as the inert concentration of the oxidant in the engine combustion process implies a considerable change in the in-cylinder thermodynamic behavior, as shown in Figure 7. Due to the higher heat capacity at constant volume of EGR vs. N_2, a lower specific heat ratio (γ) is obtained in the intake charge gas. As a consequence, lower peaks of pressure and temperature are obtained at the TDC and at the peak of combustion in the oxy-fuel combustion case. Also, as a consequence of lower γ, the indicated efficiency of the compression ignition cycle decreases; therefore, more fuel is required to produce the same torque and power for a given engine speed. Consequently, more oxygen and more EGR must be trapped inside the cylinder, as shown in Figure 7, i.e., the trapped mass for the same power is higher in the oxy-fuel combustion mode. It is worth noting that the effect of lower gamma of the EGR vs. The N_2 is so strong that even with higher trapped mass, the in-cylinder pressure peak in the oxy-fuel combustion is lower. Also, the effect of the lower gamma is evident in the gas temperature evolution during the expansion stroke (from TDC —angle equal to 0— to IPO) due to the lower temperature decrease from the temperature peak.

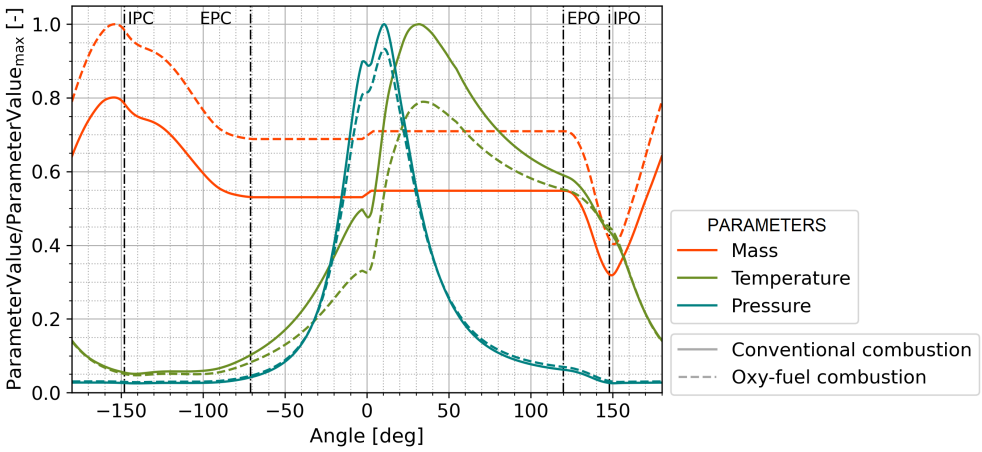

Figure 7. In−cylinder thermodynamic behavior of engine in oxy-fuel combustion compared to conventional combustion at full load engine operating point.

As a consequence of the changes produced in the chamber, the behavior of the intake and exhaust gases varies with respect to that obtained when the engine operates with air. The exhaust mass flow in the engine increases due to the higher in-cylinder trapped mass, generating more flow, which drives the turbines (TCH-1AG and TCH-2AG in Figure 2b), and therefore increasing the outlet pressure of the corresponding compressors, as reflected in Figure 8. As for the temperatures, the inlet temperature is the same in both the conventional and oxy-fuel combustion cases, since it is controlled by the coolers located after compressors to obtain a target value; on the other hand, the exhaust temperature is slightly lower in the oxy-fuel combustion case, a result of the combustion temperature reduction. The lower specific heat ratio in the oxy-fuel combustion case generates a lower expansion

effect as the piston travels from TDC to BDC. This, combined with a lower peak cylinder temperature (see Figure 7), results in an exhaust gas temperature similar to that of the conventional combustion case.

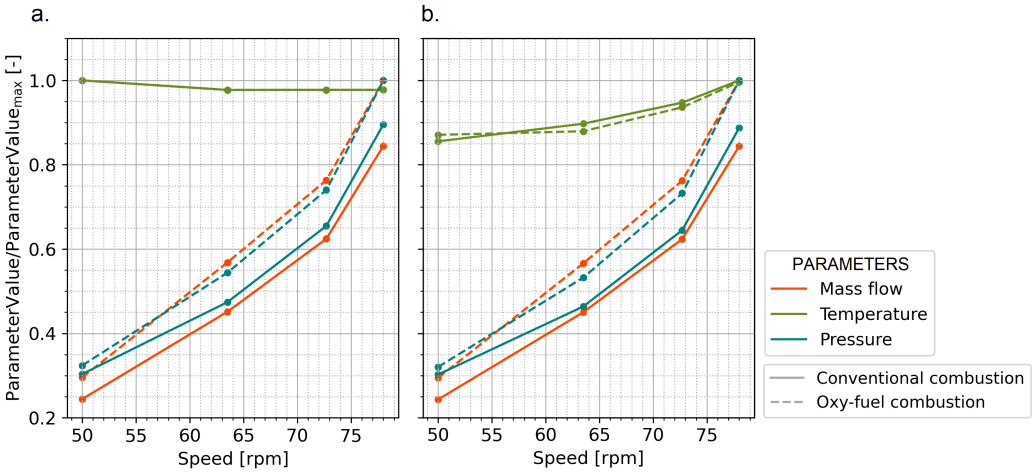

Figure 8. Engine intake and exhaust gas behavior in oxy−fuel combustion compared to conventional combustion: (**a**) intake; (**b**) exhaust.

As represented in Figure 9, where the main engine parameters have been represented, the above-mentioned phenomena impact the engine performance when running under the oxy-fuel combustion mode. The effect of the lower specific heat ratio (gamma) during the engine cycle results in less work produced per engine cycle and, therefore, in a lower indicated thermal efficiency for the same torque and power at each engine speed. Since the model control seeks to get the same reference model BMEP, the fuel demand increases to compensate for the lack of work produced, thereby increasing the Brake-Specific Fuel Consumption (BSFC).

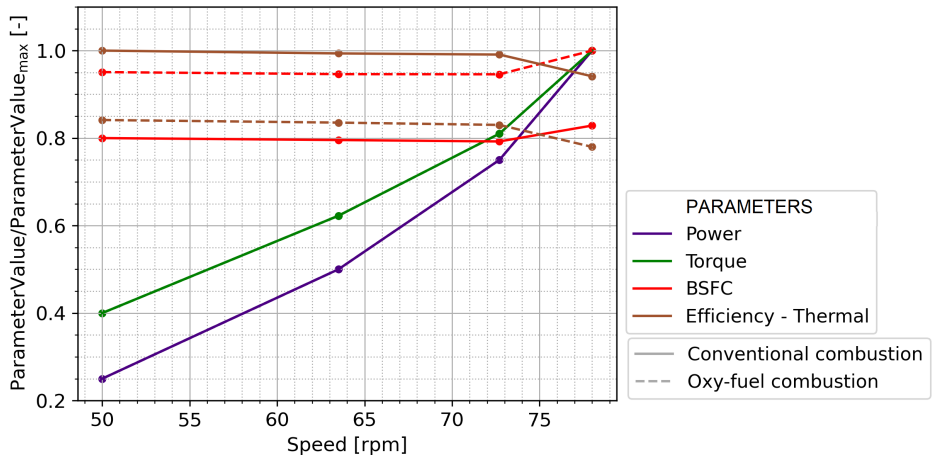

Figure 9. Engine performance curves in oxy−fuel combustion compared to conventional combustion.

3.2. O_2 Production System Design Process Results

Following the layout optimization procedure explained in the method section, the results of each turbocharging configuration are examined to select the most energy-efficient one according to the established criteria, then the selected system is adapted to operate at all engine operating points to finally evaluate the heat exchanger network and analyze the membrane area sweep on the conclusive layout.

3.2.1. Turbocharging System

Figure 10 presents the effect of the turbocharger size ratio on the turbocharger behavior (summarized in Table 3), and Figure 11 shows the resulting air conditions at the MIEC membrane and the mass fuel consumption in the burners for each turbocharging configuration. The graphs are intended to be read from right to left, as the sweep was carried out by downsizing the second turbocharger, as explained in the Method section of this document. The bottom axis of the graphs is the turbine scale factor, which is the same as that of the full turbocharger, since no further correction is required, as opposed to for the compressor. The upper axis is the corresponding scale factor of the compressor with respect to the original size, after adjusting its corrected mass flow factor. Scale factors are in percentage; therefore, 100% means that the turbomachinery has equal size to the original engine turbochargers, while lower values mean that the turbomachinery size—maximum diameters—has been reduced. Finally, to facilitate the analysis of Figure 11a, the blue vertical dash-dot line points out the turbocharger size ratio that consumes the least fuel.

- *Parallel configuration* (Figure 4): When the turbochargers are connected in parallel, the turbines share the N_2 inlet line, so it must be divided so that each receives a part of the flow. If the turbines are of the same size, both suck in equal amounts of N_2, but if one of them is smaller, the N_2 intake flow will be reduced. This characteristic in parallel arrangement explains the evolution of the behavior in the turbochargers when performing the size sweep of the TCH-2NA turbo (see Figure 10c). The TCH-1NA turbocharger has a predictable tendency, as the higher the N_2 corrected mass flow through the turbine, the higher the speed, power, and pressure ratio of the turbine and compressor; however, the same is not true for the TCH-2ON turbocharger, because there are other factors aside from the N_2 mass flow, affecting its performance. As Table 3 presents, the pressure ratio in TCH-2ON turbine increases because the rise in the pressure ratio in the TCH-1NA compressor leads to a higher pressure of N_2 flowing out of the MIEC. However, its temperature is lower due to the drop in fuel consumption (see Figure 11a); as a result of these conditions in the N_2 coming out of the MIEC, the THC-2ON turbocharger power decreases.
  After this analysis of turbocharging variation, it is possible to explain the effect on MIEC operation and fuel burner expenditure in parallel configuration (Figure 11a). The increase in power and pressure ratio of TCH-1NA turbocharger entails an increase in the air mass flow coming in the system and in the air pressure after compression, thus contributing to the increment in the O_2 partial pressure on the feed side. On the other hand, the decrease in THC-2ON turbocharger power causes a lower suction in the O_2 flow line and and thus leads to to a higher O_2 partial pressure on the permeate side. Despite the latter, the ratio of O_2 partial pressures in the MIEC increases because the growth rate of the partial pressure on the feed side is higher than on the permeate side until it reaches 10% of the turbine scale factor, beyond which the tendency is the opposite. The lowest fuel consumption appears at around 12.5% of the TCH-2NA turbine scale factor, in the range where the ratio of O_2 partial pressures is the maximum, and within this, where the temperature of the air entering the MIEC is higher.
- *Serial configuration* (Figure 5): When the turbochargers are placed in series, the larger one (low-pressure turbine) always receives all the N_2 flow entering the turbocharging system, while the smaller one (high-pressure turbine) could be bypassed to regulate the flow boosting the turbine and thus to avoid working out of range. In this case, the TCH-2ON turbocharger is bypassed, for which a sweep of the valve lift with respect to the turbine scale factor was performed to establish the lift that produces the lowest fuel consumption. Figure 12 displays this sweep for openings between 20% and 60%, since in this interval the turbocharger works properly. As can be seen, the lifts from 40% to 60% are very close and produce the lowest fuel consumption, independently of the turbine scale factor, so the selected one is 50% to avoid being at the limit of the range.

Continuing with the analysis of the serial turbocharging system, as the N_2 mass flow through TCH-2ON turbine decreases by its size reduction, there is less suction in the N_2 line leaving the MIEC, thus slightly decreasing the mass flow passing through the TCH-1NA turbine; for this reason, the behavior of the TCH-1NA turbocharger is opposite to that manifested by the parallel arrangement. As for the TCH-2ON turbocharger, examining Figure 10b and Table 3, it is evident that the pressure ratio in the turbine increases even though the inlet pressure decreases, which occurs because the outlet pressure also drops, but at a higher rate. This increment in the pressure ratio and temperature of the flow entering TCH2-ON turbine results in an increase in the power output of the TCH-2ON turbocharger.

Table 3. Summary of curve trends in Figure 10 as scale size factors of TCH-2NA turbine decrease.

Element	Parameter	Parallel	Serial	Two Stages
TCH-1 Turbocharger	All except Temperature IN	↖	↙	↙
TCH-2 Compressor	Corr. mass flow	↙	↖	↙
	Pressure ratio	↙	↖	↖
	Power	↙	↖	↖
TCH-2 Turbine	Corr. mass flow	↙	↙	↙
	Pressure ratio	↖	↖	↖
	Pressure IN	↖	↙	↖
	Pressure OUT	=	↙	↙
	Temperature IN	↙	↖	↖
	Power	↙	↖	↖

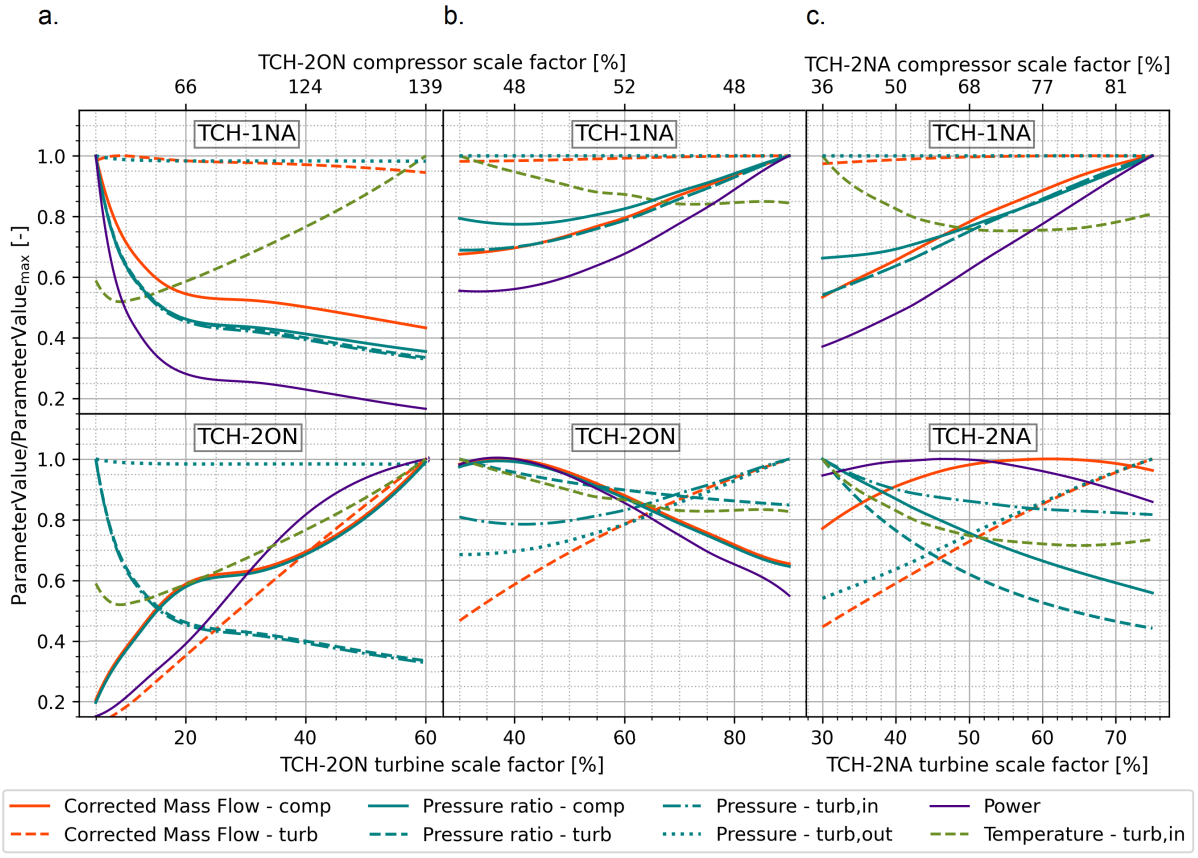

Figure 10. Influence of turbocharger size ratio on turbocharger behavior in the configurations studied at full load engine operating point. (**a**) Parallel; (**b**) serial; (**c**) two−stage compression.

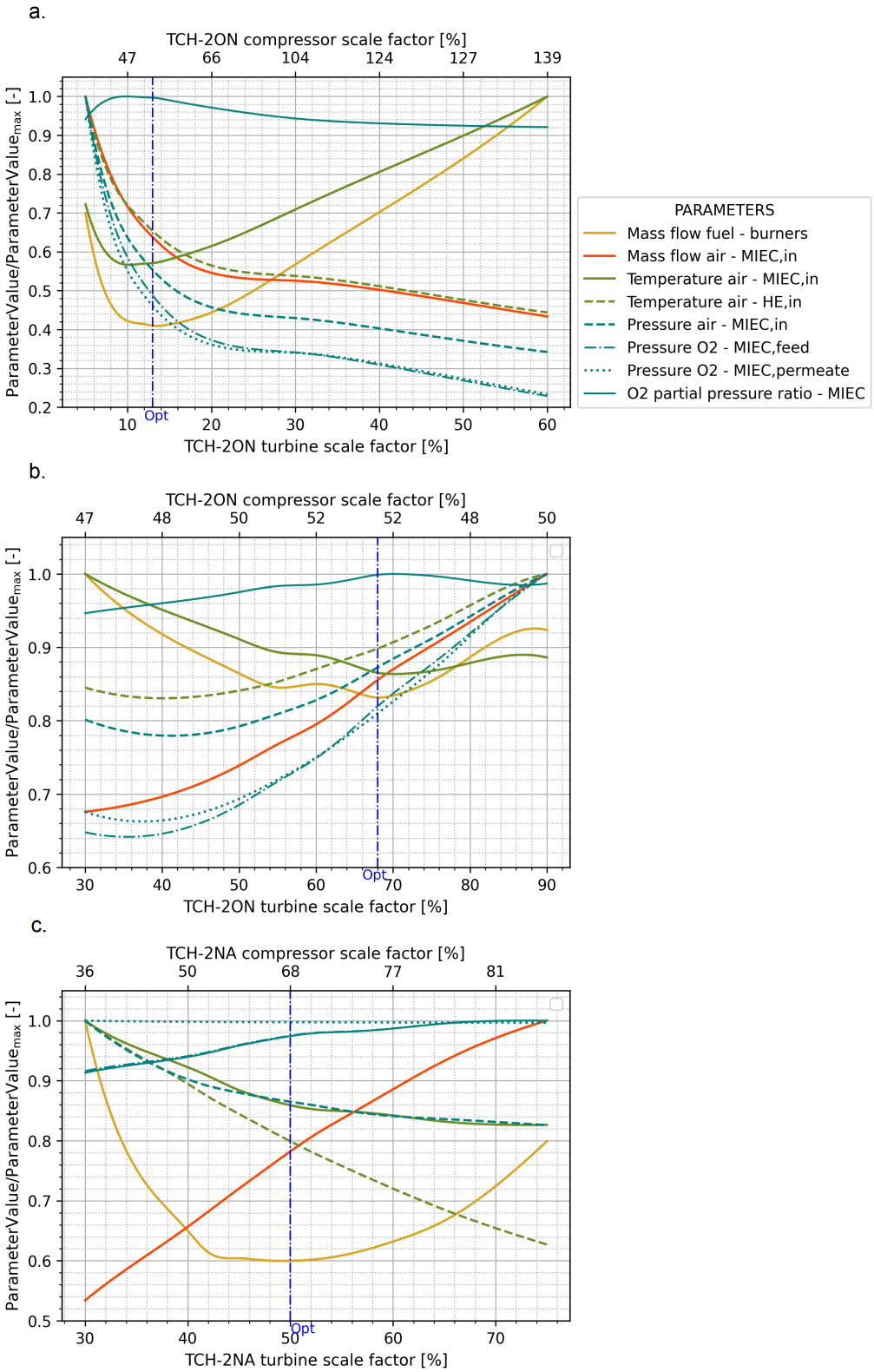

Figure 11. Influence of turbocharger size ratio on MIEC operating conditions and burner fuel consumption in the configurations studied at full load engine operating point. (**a**) Parallel; (**b**) serial; (**c**) two−stage compression.

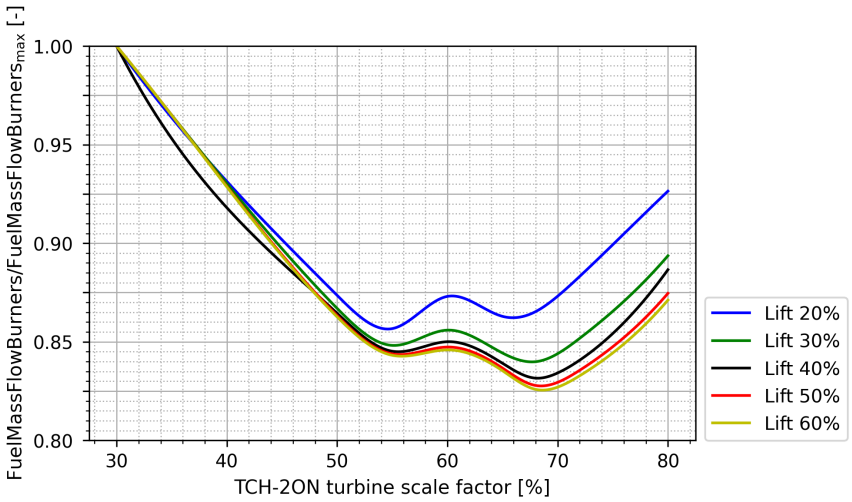

Figure 12. Sweep of the bypass valve lift of the serial turbocharging system.

Regarding the MIEC operating conditions and fuel consumption, the decreased performance of TCH-1NA turbocharger implies a decrease in the air mass flow drawn from the atmosphere and in the air pressure after compression, leading to a lower O_2 partial pressure on the membrane feed side. The improved power of TCH-2ON generates a higher vacuum in the O_2 flow line and, consequently, a decrease in the O_2 partial pressure on the permeate side. Despite the decrease in O_2 partial pressures on both membrane sides, the ratio between them depends on the rate of decrease of one with respect to the other. As evidenced in Figure 11b, from 72% to 68% of turbine scale factor, the slopes of both curves are almost equal, and from the last point, the slope of the partial pressure on the feed side is greater than on the permeate; for this reason, the O_2 partial pressure ratio increases up to this range and then decreases. The lowest fuel consumption is found at 68% of the TCH-2NA turbine scale factor, in the range where the ratio of O_2 partial pressures is the maximum, and within this, where the temperature of the air entering the MIEC is higher, as concluded in the parallel configuration.

- *Two-stage air compression* (Figure 6): The third turbocharging configuration studied is another serial arrangement but, in this case, the two turbochargers work in full serial mode (i.e., no bypass valve) and both are located in the air flow line to obtain the O_2 partial pressure gradient in the MIEC by compressing only the fluid going to the feed side. Since this configuration has the operating principle of the previous one, the TCH-1NA turbo has the same tendency in performance variation (Figure 10c). Nevertheless, the TCH-2NA turbocharger power first improves due to the increase in the pressure ratio and temperature of N_2 entering TCH-2NA turbine, but later decreases due to the corrected mass flow decrease. It is worth noting that, this time, the pressure ratio increases due to the rise in the inlet pressure of TCH-2NA turbine caused by the conditions produced in the MIEC; in addition to the significant decrease in the inlet pressure of TCH-1NA turbine (outlet of TCH-2NA turbine).
  Although the turbocharger behavior in this case is very similar to the previous one, the MIEC and fuel consumption are different. The reason is that the cooler between the compression stages leads to a lower air temperature after the turbocharging system compared to the other designs studied (it can be seen in Figure 13), so now the main purpose of the burners is to heat the air up to the MIEC requirement instead of increasing the O_2 partial pressure ratio, because the two-stage air compression is high enough to reach a very good outlet air pressure. This change in the burner operating objective explains why the EGR line burner is not needed for this configuration at full engine load and the exhaust gas line burner is sufficient to heat the air to the required

value at the MIEC. The lowest fuel consumption is obtained when the TCH-2NA turbine scale factor is around 50%, where the temperature of air entering the MIEC is high enough without further reduction in O_2 partial pressure ratio in the MIEC.

It is important to highlight that this study relies on two main parameters related to the MIEC operation: the ratio of O_2 partial pressures between the feed and permeate side, and the temperature of air coming in the membrane. These parameters have a proportional and opposite tendency during the sweep of the scale factors, as shown in Figure 11a–c. The fuel consumption, as well as the air temperature reaching the MIEC, follows a somewhat opposite trend to the O_2 partial pressure ratio achieved by the turbocharging system, as long as the air temperature entering the heat exchanger network is not too far from what the system requires, in which case the fuel consumption will depend on the latter.

Once each turbocharging configuration has been examined, the arrangements are compared using Figure 13, which shows the main variables that define the system efficiency, in order to subsequently select the most energy-efficient one. As can be seen in the graph, the two-stage air compression configuration achieves the highest ratio of O_2 partial pressures and the highest air mass flow despite the lower temperature of the air entering the MIEC. This turbocharging layout achieves the best possible conditions for the membrane operation, which results in the lowest fuel consumption in the burners.

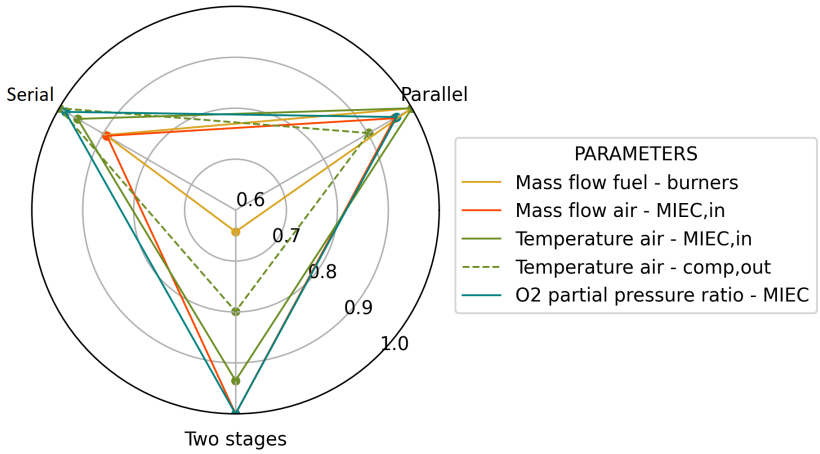

Figure 13. Comparison of turbocharging configurations studied at full load engine operating point.

Before continuing with the heat exchanger network evaluation and the membrane area sweep, the selected turbocharging configuration is evaluated for all engine speeds. As can be seen in Figure 14a, the intake air mass flow entering the MIEC is almost constant for the first three operating points, regardless of the O_2 target for each of them. In this range, the trends of the air temperature and O_2 partial pressure ratio are opposite to that shown in Figure 11c, but this time the fuel consumption in the burners is proportional to the latter because the size of the turbochargers is the same, and therefore the decisive parameter is the temperature. At full load, the air mass flow increases because the growth of the air temperature with respect to the preceding point is not significant, and the other parameters must compensate for the MIEC requirements to generate the O_2.

Figure 14b–e show the compressor and turbine maps for the optimum size found of turbochargers TCH-1NA and TCH-2NA for all engine operating points. In these, confirming the previous explanation, the first three engine speeds are very close (indeed, 72.7 rpm points overlaps 63.5 point in the turbocharger maps) and the full load point presents more pressure ratio and reduced mass flow.

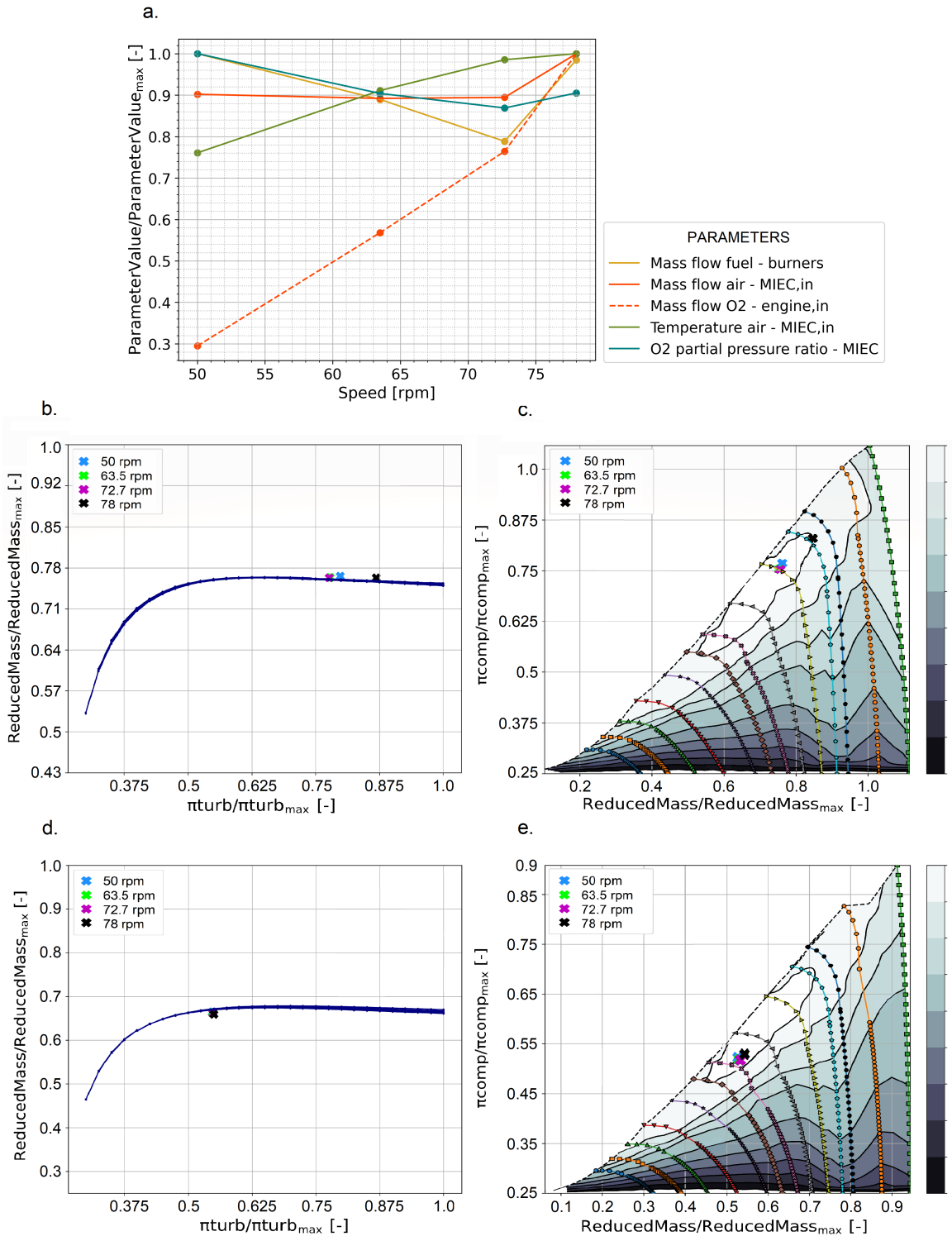

Figure 14. Two−stage air compression configuration evaluated at all engine operating points: (**a**) MIEC operating conditions and burner fuel consumption; (**b**) turbine map of TCH-1NA; (**c**) compressor map of TCH-1NA; (**d**) turbine map of TCH-2NA; (**e**) compressor map of TCH-2NA.

3.2.2. Heat Exchanger System

The heat exchanger network was conceived on the basis of previous studies and adapted to the marine engine conditions, as explained in the Method section. Its optimization process was oriented to take advantage of the residual energy from the fluids circulating in the O_2 production system by using as few regenerators as viable. In this way,

the heat exchanged by each regenerator is the criteria utilized to discard the less necessary ones and thereby obtain the most simplified heat exchanger network.

Figure 15a first shows a bar chart of the heat exchanged in each regenerator as the ratio over the total heat exchanged in the network, for the most optimal turbocharging system selected and for the full engine operating point; this chart also represents the hot and cold fluids passing through each regenerator. Secondly, Figure 15b shows the same as the previous one but for all engine operating points, so a typical line graph is used instead of a bar chart. Both are in logarithmic scale for representation purposes due to the different orders of magnitude in heat exchange.

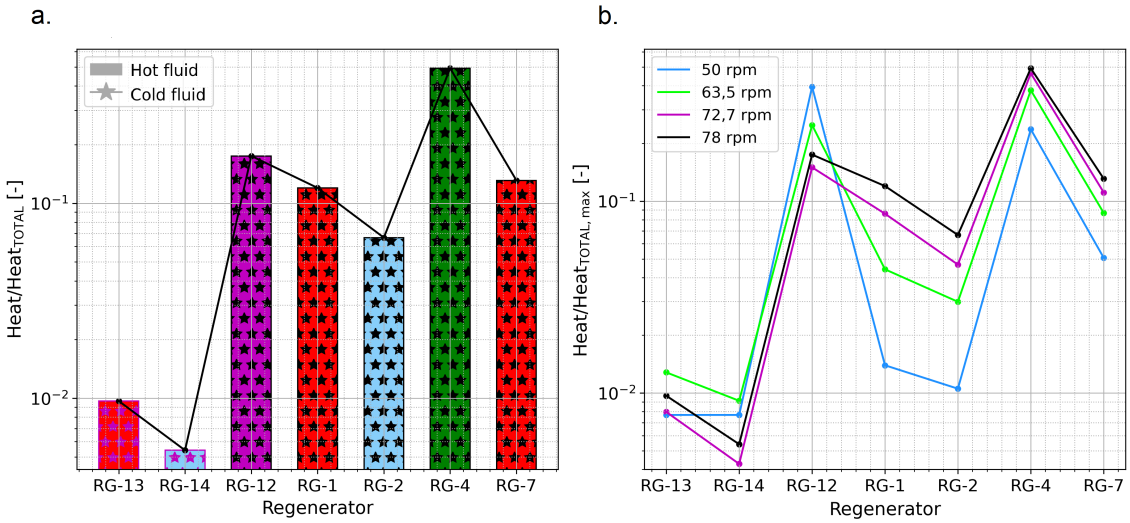

Figure 15. Heat exchanged in the regenerators of the two−stage air compression configuration. The bars are arranged following the heat transfer order of the flows. (**a**) Full load engine operating point. The color coding of the fluids is the same as in the O_2 production system diagram of Figure 6. (**b**) All engine operating points.

As reflected in the first graph, N_2 (RG-4) is the fluid that contributes the most to air warming, followed by engine exhaust gases (RG-7); both account for almost three-quarters of the total energy transferred to the air. On the other hand, the O_2 line (RG-14) provides the least energy to the air; however, its heat input helps more to reduce the fuel consumption necessary to heat up the EGR at low loads, and thus add the missing energy to the air in order to meet the MIEC requirements. Although the regenerators that heat the EGR before it transfers energy to the air (RG-13 and RG-14) present much less heat transferred than the other regenerators, they contribute more at low loads to the reduction in fuel consumption in the burners, in addition to cooling the O_2 and exhaust gases to facilitate the following processes involving these fluids, as explained in the Method section.

When evaluating the heat exchanger network at the other engine operating points (Figure 15b), it is observed that as engine load decreases, the heat transferred to the air by the exhaust gases also decreases because the mass flow and the energy available in this fluid is proportional to the engine load. Since the O_2 demand by the engine decreases with the engine speed, the operating requirements from the MIEC change and the heat exchanged between the gases leaving the MIEC and the intake air declines. As a result of the loss of energy available in these flow lines, the EGR needs to transfer a larger share of heat to the air to meet the MIEC requirements. As a result, the heat transferred by the EGR (RG-12) increases for the operating points with the lowest speed, which translates into an increased fuel consumption that burns with the excess O_2 from the EGR.

3.2.3. MIEC Membrane

Once the final O_2 production system is established and evaluated for all engine operating points, the membrane area sweep is performed to select the most suitable one for the final design. Figure 16 shows the ratio of fuel used in the burners to engine fuel consumption for each area evaluated. Modifying the membrane surface area leads to a better permeability since it favors the adsorption and dissociation of oxygen molecules by reducing the resistance of their transport through the membrane; for this reason, larger membranes require less pressure and temperature to operate [25]. The tendency of curves is asymptotic, which means that from a specific membrane area onward, its increase does not bring about significant improvements in fuel consumption; this phenomenon occurs as there are certain minimum air requirements (temperature, pressure) for the membrane to operate.

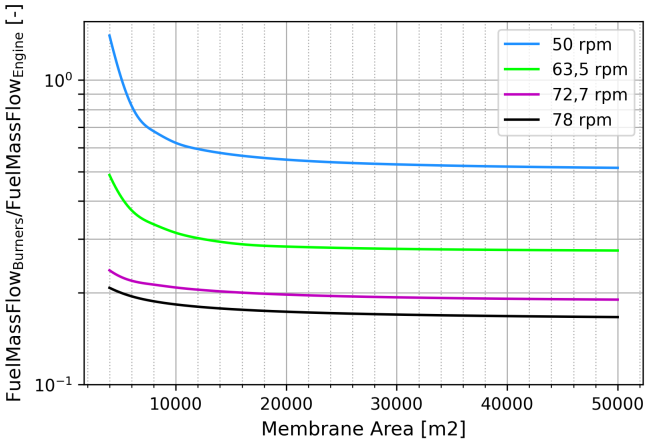

Figure 16. Membrane area sweep of the two−stage air compression configuration.

Regarding the differences in fuel consumption between the engine operating points, the points at lower engine speed present a higher relative fuel consumption. This is mainly due to the fact that the flow lines of the O_2 production system coming from the engine transfer much less heat to the incoming air than at higher engine speeds. Based on this analysis, the membrane area selected considering all engine operating points is 14,000 m^2.

3.3. Conclusive Oxy-Fuel Marine Engine Layout

Figure 17 shows the complete final configuration of the marine engine working with oxy-fuel combustion and connected to the in situ O_2 production system obtained from the optimization process. The actual values from the simulations correspond to full load conditions (78 rpm) and are the ones shown in the schematic, since the analysis of the ongoing study results was performed with relative values to protect the engine manufacturer's data. In the diagram, this information is still secured, because it only shows flow data for the engine operating under oxy-combustion conditions.

It is important to comment that the exhaust gases leaving the engine configuration, i.e., the TCH-1AG turbocharger, present a very low temperature of 276.8 °C compared to an automotive engine. After the CC-2 burner, this temperature rises to 1212.3 °C, but since the mass flow after the flow splitting is low (5.8 kg/s), the heat transferred to the air is not sufficient, as discussed in the heat exhanger system analysis. At the end of the exhaust gases' path, the temperature achieved is 280.1 °C for the subsequent CO_2 capture process. On the other hand, the EGR mass flow is 48.3 kg/s, which is much higher than the exhaust gas mass flow due to the EGR-to-O_2 ratio established at the beginning of this study. For the exposed engine operating point (78 rpm), the CC-3 burner is not used, as explained in the turbocharging system selection. For this reason, the EGR temperature before transferring the heat energy to the air is 282.7 °C, almost the same as the initial 274.5 °C. Finally, with respect to O_2 production, since combustion in four cylinders (half of the engine) requires 4.5 kg/s of O_2, the air conditions reached at the MIEC for this purpose are as follows:

air temperature of 802.1 °C, air mass flow of 39.7 kg/s, air feed pressure of 7.2 bar, and therefore an O_2 partial pressure ratio of 1.06.

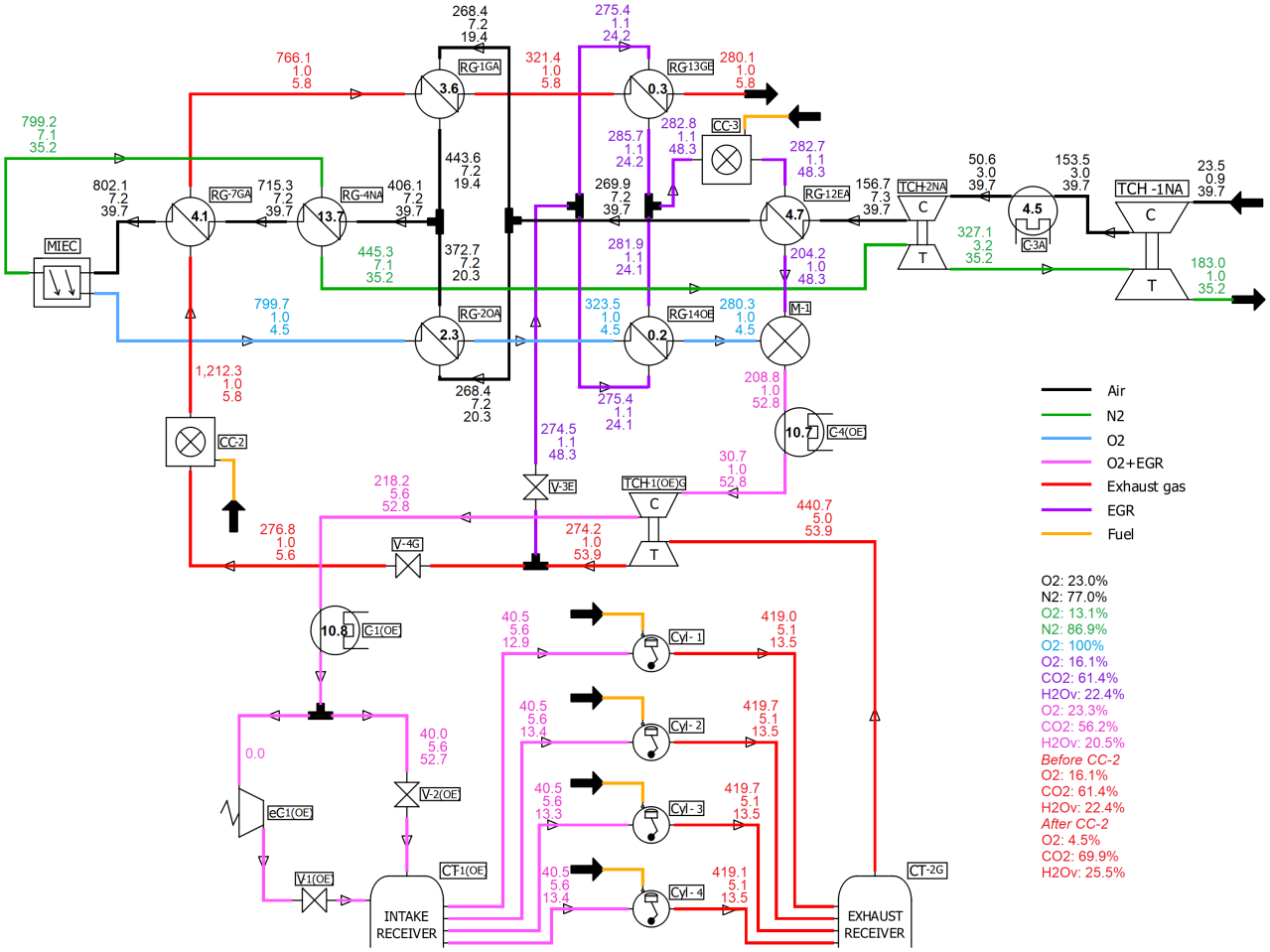

Figure 17. Conclusive and complete schematic of the oxy-fuel marine engine showing the actual values from simulations at full load engine operating point (78 rpm). (**Top**) Temperature (°C). (**Medium**) Pressure (bar). (**Bottom**) Mass flow (kg/s). (**Inside and bold**) Power (MW).

4. Conclusions

To the best of the authors' knowledge, this is the first detailed study available in the literature about oxy-fuel combustion in a 2S multi-cylinder cargo ship engine where, additionally, turbocharging, oxygen generation, and exhaust gases post-combustion conditioning sub-systems have been considered for the succeeding CO_2 capture process.

The oxy-fuel combustion technology is a novel option for exhaust gas treatment in maritime transport, as it avoids NO_x emissions and facilitates the separation of CO_2 from exhaust gases for subsequent capture. However, these improvements in emissions levels come at the expense of increased engine BSFC to obtain the original brake power and torque. This is because EGR, by replacing N_2 in the intake charge, has a lower specific heat ratio, which decreases the indicated efficiency per cycle and thus increases fuel consumption.

In situ O_2 production in a marine engine is seen as a convenient solution for the implementation of oxy-fuel combustion onboard vessels due to the logistic hassle that supplying large amounts of O_2 from an external source would imply. The O_2 production system, based in MIEC membranes, involves two main subsystems that work together to condition the air for its separation process in the membrane: a heat exchanger network and a turbocharging system.

The heat exchanger system requires the implementation of combustion chambers in the exhaust gas and EGR flow lines to increase the heat transfer to the air, because the energy obtained from the flow lines coming from the engine is not sufficient due to the thermo-mechanical limits for exhaust gas temperature in 2S marine engines. The excess O_2 present in the exhaust gas stream is used to oxidase additional fuel with a two-fold benefit: increasing the temperature of the flue gases and reducing the concentration of O_2 for an effective posterior CO_2 separation. Although limited to the two lowest engine speeds, the combustion chamber in the EGR flow line is necessary, because the available heat in the exhaust gases is lower than at full load conditions.

In relation to the turbocharging configuration selection, a 3-end design membrane was used for O_2 generation in the marine engine as it was initially assumed that the driving force to compensate for the missing sweep current in the MIEC would be a vacuum suction force on the permeate side. Nevertheless, during the evaluation of the various types of turbocharging configurations, it was concluded that the two-stage air compression system remains the best solution due to the high O_2 partial pressure achieved on the feed side, confirming the preference for it in previous related studies available in the literature.

Along with the selection of the turbocharging arrangement, it is essential to optimize the performance of the configuration itself in order to find the most optimal turbocharger size ratio to obtain the lowest fuel consumption in burners. To this end, the present work proposes a methodology that consists of maintaining the size of the turbocharger that receives the air directly from the atmosphere equal to that of the air engine design, while sweeping the second turbocharger size with respect to this reference one. This methodology is followed because increasing the dimensions of the first turbocharger is not feasible due to its large size, and on the other hand, decreasing it implies having less air mass flow entering the complete system. Instead, downsizing the second turbocharger improves the air conditions for the MIEC membrane operation as long as it does not exceed the reduction limit beyond which the tendency is not favorable. The size scale factor sweep is in turn a two-step methodology. The first step entails using the similarity laws of turbomachinery to downsize the whole turbocharger, and even if the scale factor used affects all the turbocharger parameters (i.e., reduced speed and flow in both compressor and turbine), the main focus is in the turbine mass flow parameter optimization. The second step focuses on fixing the turbine size and modifying only the compressor size to achieve the optimal operative conditions. The output of this process is a different turbocharger size and compressor-to-turbine matching than the original turbocharger.

In order to complement the suggested technology for the purpose of reducing exhaust gas emissions in marine engines, a further research work is proposed to integrate the study of the CO_2 capture concept in the present model.

Author Contributions: Conceptualization, J.R.S., F.J.A. and A.C.; methodology, J.R.S., F.J.A. and A.C.; software, F.J.A.; validation, R.B. and A.C.; formal analysis, R.B. and A.C.; investigation, R.B.; resources, J.R.S., A.C.; data curation, F.J.A., R.B. and A.C.; writing—original draft preparation, R.B.; writing—review and editing, J.R.S., F.J.A. and A.C.; visualization, F.J.A.; supervision, J.R.S. and F.J.A.; project administration, J.R.S.; funding acquisition, J.R.S., F.J.A. and A.C. All authors have read and agreed to the published version of the manuscript.

Funding: This research has been partially supported by Grant CIPROM/2021/061 funded by Generalitat Valenciana. Also partially supported by Grant PID2021-123351OB-I00 funded by MCIN/AEI/10.13039/501100011033 and, as appropriate, by "ERDF A way of making Europe". And also partially funded by Programa de Ayudas de Investigación y Desarrollo PAID-01-22, from Universitat Politècnica de València (UPV) which granted the Rossana's pre-doctoral contract.

Institutional Review Board Statement: Not applicable.

Informed Consent Statement: Informed consent was obtained from all subjects involved in the study.

Data Availability Statement: Data available on request from the authors.

Conflicts of Interest: The authors declare no conflict of interest.

Abbreviations

The following abbreviations are used in this manuscript:

2SE	Two-Stroke Engine
BMEP	Break Mean Effective Pressure
BOF	Basic Oxygen Furnace
BSCF	$Ba_{0.5}Sr_{0.5}Co_{0.8}Fe_{0.2}O_3$ membrane
BSFC	Brake-Specific Fuel Consumption
CAC	Compressed Air Cooler
C- #A	Cooler- #Air
C- #E	Cooler- #EGR
C- #O	Cooler- #Oxygen
C- #(OE)	Cooler- #Oxygen+EGR mixture
C-ASU	Cryogenic Air Separation Unit
CC- #O	Combustion Chamber- #
CCS	Carbon Capture and Storage
CI	Compression Ignition
CMCR	Contracted Maximum Continuous Rated
CO_2	Carbon Dioxide
CT- #A	Collector of Air pipes #
CT- #G	Collector of exhaust Gas pipes #
CT- #(OE)	Collector of Oxygen+EGR mixture pipes #
Cyl- #	Cylinder- #
DPF	Diesel Particulate Filter
eC- #A	Compressor (booster) electrically driven- #Air
eC- #(OE)	Compressor (booster) electrically driven- #Oxygen+EGR mixture
ECA	Emission Control Areas
EGR	Exhaust Gas Recirculation
GHG	Greenhouse Gas
HFO	Heavy Fuel Oil
HVOF	High Velocity Oxy-Fuel
IMO	International Maritime Organization
m/m	mass by mass
M- #	Mixer of gases- #
MARPOL	Marine and Pollution
MDO	Marine Diesel Oil
MIEC	Mixed Ionic–Electronic Conducting Membrane
N_2	Nitrogen
NOx	Nitrous Oxides
O_2	Oxygen
ODS	Ozone Depleting Substances
PM	Particulate Matter
RG- #EA	Non-mixing Heat Regenerator- #EGR-Air
RG- #EE	Non-mixing Heat Regenerator- #EGR-EGR
RG- #GA	Non-mixing Heat Regenerator- #exhaust_Gas-Air
RG- #GE	Non-mixing Heat Regenerator- #exhaust_Gas-EGR
RG- #NA	Non-mixing Heat Regenerator- #Nitrogen-Air
RG- #OA	Non-mixing Heat Regenerator- #Oxygen-Air
RG- #OE	Non-mixing Heat Regenerator- #Oxygen-EGR
SCR	Selective Catalytic Reduction
SOx	Sulfur Oxides
TCH- #AG	Turbocharger- #Air-exhaust_Gas
TCH- #NA	Turbocharger- #Nitrogen-Air
TCH- #ON	Turbocharger- #Oxygen-Air
TCH- #(OE)G	Turbocharger- #Oxygen+EGR mixture-exhaust Gas
V- #E	Regulation Valve- #EGR

V- #G	Regulation Valve- #exhaust Gas
V- #(OE)	Regulation Valve- #Oxygen+EGR mixture
VGT	Variable Geometry Turbine
VEMOD	Virtual Engine Model

References

1. International Maritime Organization. Marine Environment. Available online: https://www.imo.org/en/OurWork/Environment/Pages/Default.aspx (accessed on 15 March 2023).
2. International Maritime Organization. Introduction to IMO. Available online: https://www.imo.org/en/About/Pages/Default.aspx (accessed on 15 March 2023).
3. International Maritime Organization. Nitrogen Oxides (NOx)—Regulation 13. Available online: https://www.imo.org/en/OurWork/Environment/Pages/Nitrogen-oxides-(NOx)-Regulation-13.aspx (accessed on 17 March 2023).
4. International Maritime Organization. Initial IMO GHG Strategy. Available online: https://www.imo.org/en/MediaCentre/HotTopics/pages/reducing-greenhouse-gas-emissions-from-ships.aspx (accessed on 20 March 2023).
5. Deng, J.; Wang, X.; Wei, Z.; Wang, L.; Wang, C.; Chen, Z. A review of NOx and SOx emission reduction technologies for marine diesel engines and the potential evaluation of liquefied natural gas fuelled vessels. *Sci. Total Environ.* **2021**, *766*, 144319 . [CrossRef] [PubMed]
6. Aakko-Saksa, P.T.; Lehtoranta, K.; Kuittinen, N.; Järvinen, A.; Jalkanen, J.-P.; Johnson, K.; Jung, H.; Ntziachristos, L.; Gagné, S.; Takahashi, C.; et al. Reduction in greenhouse gas and other emissions from ship engines: Current trends and future options. *Prog. Energy Combust. Sci.* **2023**, *94*, 101055. [CrossRef]
7. Einbu, A.; Pettersen, T.; Morud, J.; Tobiesen, F.; Jayarathna, C.; Skagestad, R.; Nysæter, G. Onboard CO_2 Capture From Ship Engines. *SSRN Electron. J.* **2021** . [CrossRef]
8. Mignard, D.; Pritchard, C. Processes for the Synthesis of Liquid Fuels from CO_2 and Marine Energy. *Chem. Eng. Res. Des.* **2006**, *84*, 828–836. [CrossRef]
9. Li, X.; Peng, Z.; Pei, Y.; Ajmal, T.; Rana, K.J.; Aitouche, A.; Mobasheri, R. Oxy-fuel combustion for carbon capture and storage in internal combustion engines—A review. *Int. J. Energy Res.* **2022**, *46*, 505–522. [CrossRef]
10. Buhre, B.J.P.; Elliott, L.K.; Sheng, C.D.; Gupta, R.P.; Wall, T.F. Oxy-fuel combustion technology for coal-fired power generation. *Prog. Energy Combust. Sci.* **2005**, *31*, 283–307. [CrossRef]
11. Wei, X.; Manovic, V.; Hanak, D.P. Techno-economic assessment of coal- or biomass-fired oxy-combustion power plants with supercritical carbon dioxide cycle. *Energy Convers. Manag.* **2020**, *221*, 113143. [CrossRef]
12. Blomen, E.; Hendriksa, C.; Neele, F. Capture technologies: improvements and promising developments. *Energy Procedia* **2009**, *1*, 1505–1512. [CrossRef]
13. Escudero, A.I.; Espatolero, S.; Romeo, L.M. Oxy-combustion power plant integration in an oil refinery to reduce CO_2 emissions. *Int. J. Greenh. Gas Control* **2016**, *45*, 118–129. [CrossRef]
14. Carpenter, S.M.; Long, H.A. Integration of carbon capture in IGCC systems. In *Integrated Gasification Combined Cycle (IGCC) Technologies*; Woodhead Publishing: Sawston, UK, 2017; pp. 445–463. [CrossRef]
15. Carrasco-Maldonado, F.; Spörl, R.; Fleiger, K.; Hoenig, V.; Maier, J.; Scheffknecht, G. Oxy-fuel combustion technology for cement production - State of the art research and technology development. *Int. J. Greenh. Gas Control* **2016**, *45*, 189–199. [CrossRef]
16. Biyiklioğlu, O.; Tat, M.E. Tribological assessment of NiCr, Al_2O_3/TiO_2, and Cr_3C_2/NiCr coatings applied on a cylinder liner of a heavy-duty diesel engine. *Int. J. Engine Res.* **2021**, *22*, 2267–2280. [CrossRef]
17. Quader, M.A.; Ahmed, S.; Ghazilla, R.A.R.; Ahmed, S.; Dahari, M. A comprehensive review on energy efficient CO_2 breakthrough technologies for sustainable green iron and steel manufacturing. *Renew. Sustain. Energy Rev.* **2015**, *50*, 594–614. [CrossRef]
18. Wu, F.; Argyle, M.D.; Dellenback, P.A.; Fan, M. Progress in O_2 separation for oxy-fuel combustion—A promising way for cost-effective CO_2 capture: A review. *Prog. Energy Combust. Sci.* **2018**, *67*, 188–205. [CrossRef]
19. Panesar, R.; Lord, M.; Simpson, S.; White, V.; Gibbins, J.; Reddy, S. Coal-Fired Advanced Supercritical Boiler/Turbine Retrofit with CO_2 capture. In Proceedings of the 8th International Conference on Greenhouse Gas Control Technologies, Trondheim, Norway, 19–22 June 2006.
20. Portillo, E.; Alonso-Fariñas, B.; Vega, F.; Cano, M.; Navarrete, B. Alternatives for oxygen-selective membrane systems and their integration into the oxy-fuel combustion process: A review. *Sep. Purif. Technol.* **2019**, *229*, 115708. [CrossRef]
21. Baumann, S.; Serra, J.M.; Lobera, M.P.; Escolástico, S.; Schulze-Küppers, F.; Meulenberg, W.A. Ultrahigh oxygen permeation flux through supported $Ba_{0.5}Sr_{0.5}Co_{0.8}Fe_{0.2}O_{3-\delta}$ membranes. *J. Membr. Sci.* **2011**, *377*, 198–205. [CrossRef]
22. Bouwmeester, H.J.M.; Burggraaf, A.J. Chapter 10 Dense ceramic membranes for oxygen separation. *Membr. Sci. Technol.* **1996**, *4*, 435–528. [CrossRef]
23. Plazaola, A.A.; Labella, A.C.; Liu, Y.; Porras, N.B.; Tanaka, D.A.P.; Annaland, M.V.S.; Gallucci, F. Mixed ionic-electronic conducting membranes (MIEC) for their application in membrane reactors: A review. *Processes* **2019**, *7*, 128. [CrossRef]
24. Shao, Z.; Yang, W.; Cong, Y.; Dong, H.; Tong, J.; Xiong, G. Investigation of the permeation behavior and stability of a $Ba_{0.5}Sr_{0.5}Co_{0.8}Fe_{0.2}O_{3-\delta}$ oxygen membrane. *J. Membr. Sci.* **2000**, *172*, 177–188. [CrossRef]

25. Interreg North-West Europe. RIVER—Non-Carbon River Boat Powered by Combustion Engines. Available online: https://vb.nweurope.eu/projects/project-search/river-non-carbon-river-boat-powered-by-combustion-engines/ (accessed on 30 March 2023).
26. Interreg North-West Europe. Oxygen Production on the CRT Narrowboat in River. Available online: https://www.opteam-network.com/critt/river0220/ (accessed on 12 July 2023).
27. Interreg North-West Europe. Installation and Integration of an Oxyfuel Combustion Engine System with CO_2 Capture and Storage Facilities on a Ship. Available online: https://opteam-network.com/critt/river0920/ (accessed on 12 July 2023).
28. Mobasheri, R.; Izza, N.; Aitouche, A.; Peng, J.; Bakir, B. Investigation of Oxyfuel Combustion on Engine Performance and Emissions in a DI Diesel HCCI Engine. In Proceedings of the 8th International Conference on Systems and Control, Marrakech, Morocco, 23–25 October 2019.
29. Martin, J.; Arnau, F.; Piqueras, P.; Auñon, A. Development of an Integrated Virtual Engine Model to Simulate New Standard Testing Cycles. In Proceedings of the WCX World Congress Experience, Detroit, MI, USA, 10–12 April 2018.
30. WIN GD Engine Types. Available online: https://www.wingd.com/en/engines/engine-types/ (accessed on 5 September 2023).
31. General Technical Data (GTD). Available online: https://www.wingd.com/en/engines/general-technical-data-(gtd)/ (accessed on 5 September 2023).
32. Ditaranto, M.; Hals, J. Combustion instabilities in sudden expansion oxy–fuel flames. *Combust. Flame* **2006**, *146*, 493–512. [CrossRef]
33. Serrano, J.R.; Arnau, F.J.; García-Cuevas, L.M.; Farias, V.H. Oxy-fuel combustion feasibility of compression ignition engines using oxygen separation membranes for enabling carbon dioxide capture. *Energy Convers. Manag.* **2021**, *247*, 114732. [CrossRef]